# Structural Predictions of the Binding Site Architecture for Monoclonal Antibody NC6.8 Using Computer-Aided Molecular Modeling, Ligand Binding, and Spectroscopy

Malini Viswanathan,* Jerry M. Anchin,‡ P. R. Droupadi,‡ Chhabinath Mandal,‡ D. Scott Linthicum,‡ and Shankar Subramaniam*

*Department of Physiology and Biophysics, Beckman Institute, University of Illinois, Urbana, Illinois 61801, and ‡Department of Veterinary Pathobiology, College of Veterinary Medicine, Texas A&M University, College Station, Texas 77843 USA

ABSTRACT Monoclonal antibody NC6.8 binds the superpotent sweetener ligand *N*-(*p*-cyanophenyl)-*N'*-(diphenylmethyl) guanidineacetic acid with high affinity ($K_d$ = 53 nM). Using computer-aided molecular modeling and several experimental techniques, such as competitive ligand binding, absorbance spectroscopy, and fluorescence spectroscopy, we have predicted the structure of the variable domain fragment (Fv) and identified the key residues in the combining site of the antibody. We have identified nine specific amino acids as being involved in ligand recognition and complexation. Most notable are H:33W, which is responsible for ligand-induced tryptophan fluorescence quenching, H:56R, which forms a salt bridge with the carboxylate moiety of the ligand, and L:34H, which, deep in the binding site, interacts with the cyanophenyl portion of the ligand. Two residues located deep in the putative binding pocket, H:35E and H:50E, provide the negatively charged potential for interaction with the protonated aryl nitrogen and the positive guanidinium group. These modeling predictions were made before the solution of high-resolution structures of the native Fab (2.6 Å) and the Fab–ligand complex (2.2 Å). Comparisons between the theoretical model and experimental native and liganded Fab structures are made.

## INTRODUCTION

Structural studies of antibody fragments have provided a basis for establishing the uniqueness of the (Ig) fold and the specificity of antigen recognition (Davies and Metzger, 1983; Davies et al., 1990; Poljak et al., 1976). The Ig fold is characterized by the β-barrel topology of each of the domains, combined with a high degree of conservation in specific packing residues, β-strand turns, and overall interdomain packing geometry (Chothia et al., 1985; Padlan, 1990; Tramontano and Lesk, 1992). The two polypeptide chains, heavy (H) and light (L), contain four and two domains, respectively, and associate through a disulfide link and numerous nonbonded hydrophobic contacts. In addition to a common fold topology, all Ig have the antigen-combining site located at the *en face*, or *N*-terminal, portion of the molecule, where the β strands form turns. The frequencies of specific residues in these loops or turns are more variable between antibodies than those for the remainder of the molecules. Such "hypervariable residues" appear to determine much of the antigen specificity of a given antibody and are termed the complementarity-determining regions (CDR).

Given these highly conserved structural and functional motifs, computer-aided molecular modeling (CAMM) antibody fragment structures from the amino acid sequence has become possible. There have been numerous efforts in the past decade that reflect this approach (Bruccoleri et al., 1988; Chothia & Lesk, 1987; Chothia et al., 1989; Chothia et al., 1986; de la Paz et al., 1986). All the methods employed for modeling antibody structures have been knowledge based. The basic theme in these methods has been to compare the antibody sequence to be modeled with those antibody sequences whose three-dimensional structures are available. The antibody with the highest sequence homology is then chosen as the scaffold for homology modeling the antibody whose structure is desired. Various refinement schemes are then used on the initial model that is formed by combination of replacement, addition, and deletion on the scaffold structure.

The primary difficulty in CAMM lies in the CDR loops themselves, because they exhibit great variation in size and composition between different antibodies. A powerful approach for modeling the loops has been developed by Bruccoleri and co-workers (Bruccoleri and Karplus, 1987; Bruccoleri et al., 1988). CONGEN, a conformational search algorithm developed by Bruccoleri et al., has been able to calculate low-energy loop configurations of Fv fragments of McPC603 and HyHEL-5 (Bruccoleri et al., 1988) and ANO2 (Bassolino-Klimas et al., 1993); these models agree well with known crystal structures. In this approach, first the loops are constructed on a framework using the chain closing algorithm of Go and Scheraga and then a systematic conformational search of the backbone torsions on a grid is carried out. For loop reconstruction, the order L2, H1, L3, H2, H3, L1 has been used consistent with the rationale that loops that span the region closest to the beta barrel in the known structures shape the topology better. In the above

*Received for publication 23 December 1994 and in final form 15 March 1995.*

Address reprint requests to Dr. Shankar Subramaniam, Center for Biophysics and Computational Biology, Department of Physiology and Biophysics, Beckman Institute, University of Illinois, 405 N. Mathews Ave., Urbana, IL 61801. Tel.: 217-244-4489; Fax: 217-244-2909; E-mail: shankar@ncsa.uiuc.edu.



0006-3495/95/09/741/13 $2.00

studies the molecular mechanics calculations were carried out in vacuo, whereas Martin et al. (1989) used a modified version of CONGEN in which solvent-modified potentials are used for molecular mechanics.

An important observation concerning the antibody hypervariable regions was made by Chothia and co-workers (Chothia and Lesk, 1987; Chothia et al., 1989). Although the loop region residues are hypervariable, it was found that a few key positions in these loops have unique configurations and that these canonical residue configurations are conserved across antibodies. The canonical region constraints have been used in modeling D1.3, and this results in very good agreement with the crystal structure. Canonical region constraints have also been used in modeling antimorphine and antihaloperidol antibody loops (Kussie et al., 1991; Anchin et al., 1991). For small antigen or hapten binding the large body of knowledge that can be gleaned from experimental competitive antigen binding data has been used for effective modeling of the antigen-combining sites (Jackson et al., 1992; Kussie et al., 1991; Sherman & Bolger, 1988).

We report the CAMM and prediction of the ligand binding site for monoclonal antibody NC6.8, which is specific for the superpotent sweetener *N*-(*p*-cyanophenyl)-*N'*(diphenylmethyl)guanidineacetic acid (Anchin and Linthicum, 1993). Our CAMM studies were aided by a variety of different experimental results that examined the binding of the sweetener ligand to the antibody. Results from competitive analog radioimmunoassays, pH titrations of radioligand binding, and fluorescence and absorption spectroscopy were all used to assist the CAMM studies and to identify the key residues in the combining site of the antibody. These results were directly compared with the high-resolution 2.6- and 2.2-Å Fab crystal structures of the native and complexed forms, respectively, of mAb NC6.8 recently obtained by Guddat and co-workers (Guddat et al., 1994). These studies are important to the understanding of the specificity of antibody–antigen complexes and may also shed light on the putative receptor recognition motifs for superpotent sweeteners.

## MATERIALS AND METHODS

### Computer-aided modeling and refinement

A number of different computer algorithms were used in this investigation to model and display graphically the Fv region of NC6.8. Programs ABalign and ABbuild of the ABGEN algorithm, written by us, were used to select "parent structures" and generate a first-order Fv model (C. Mandal, D. S. Linthicum, and S. Subramaniam, unpublished programs).

Each of the H- and L-chain sequences of the Fv fragment of NC6.8 is divided into seven segments, four framework (FR) regions and three CDRs. The FR segments constitute the more conserved part and have several residues that are strictly conserved or conservatively replaced. These segments form the core of the β-barrel structure. Table 1 lists the residues that are conserved in more than 95% of the Ig sequences reported in the Kabat database of Ig sequences (Kabat et al., 1991) and are also conserved in NC6.8. In as much as these residues occur at exactly the same relative position in all the immunoglobin sequences they serve as fingerprint residues to enforce alignment.

**TABLE 1 Conserved residues in immunoglobulin sequences**

| L Chain | | | H Chain | | |
|---|---|---|---|---|---|
| 5:T | 61:R | 82:D | 4:L | 86:D | 106:G |
| 6:Q | 62:F | 86:Y | 8:G | 88:A | 107:T |
| 16:G | 64:G | 88:C | 22:C | 90:Y | 110:T |
| 23:C | 65:S | 98:F | 26:G | 92:C | 111:V |
| 35:W | 73:L | 99:G | 36:W | 103:W | 112:S |
| 59:P | 75:I | 101:G | 45:L | 104:G | 102:T |

Conserved in 95–99% in known sequences (Kabat et al., 1991).

The H- (L-) chain framework scaffolds are chosen based on the highest sequence homology. Because H and L chains are aligned separately, two different parent proteins contribute chains to the scaffold. The sizes of the CDRs for the parent antibody fragments match that of NC6.8, and hence no effort was made to graft CDR fragments from other antibody structures.

The first stage in the structural modeling entails building the H–L joint chain framework scaffold from the best model chains. As the H and L chains of the test model are contributed by different parent antibody structures, the best H–L framework structural alignment was accomplished by a least-squares refinement with reference to the two parent structures. All atoms in the chains were used in the least-squares refinement.

Once the entire framework scaffold model, including H and L chain, was obtained, the residue replacements that were required was carried out. Because all these mutations in the FR region were highly conservative substitutions, no backbone refinement was carried out. The side-chain torsions of the residues replaced in the FR region were explored for the best contact and packing, defined by a strict van der Waals criterion, and the resulting model was used as the model for the framework region. More substitutions were required in the CDRs, and the resulting CDR configurations required further refinement.

### Molecular dynamics refinement

The refinement of the initial model was carried out by the use of molecular mechanics and molecular dynamics techniques. The XPLOR (Brunger et al., 1987) program was used to generate the low-energy conformations of the CDR loops. An approximate solvent screening effect was introduced by use of the distance-dependent dielectric term in the electrostatic potential term. Harmonic constraints of 50 kcal/mol Å$^2$ were applied to fix the entire framework region of the model. Chothia and Lesk (1987) observed certain canonical configurations in the CDRs among different antibodies. The CDRs of our model were examined for any of these canonical loop conformations. Distance restraints were then applied to the atoms involved in the canonical conformations for effective modeling of the loop regions. The system was subjected to 20 ps of molecular dynamics at 300 K, and configurations were obtained through quenching of trajectories at 2-ps intervals. The L- and H-chain CDRs were modeled in the order L2, H1, L3, H2, H3, and L1 as proposed by Bruccoleri and co-workers (Bruccoleri et al., 1988). Electrostatic surface renderings of the models were generated by the NCVIEW algorithm, which uses the van der Waals surface derived from the radii values compiled by Bondi (1964).

### Experimental methods used for modeling

#### *Monoclonal antibodies*

We have produced a library of monoclonal antibodies against the guanidine sweetener *N*-(*p*-cyanophenyl)-*N'*-(diphenylmethyl) guanidineacetic acid (Anchin and Linthicum, 1993). This ligand is 200,000 times more potent than sucrose as measured in a threshold taste test for sucrose (Muller et al., 1992). The structure of the ligand is depicted in Fig. 1. The immunogen was prepared by conjugation of the ligand to bovine serum albumin through the paraposition of one of the phenyl rings; this material was

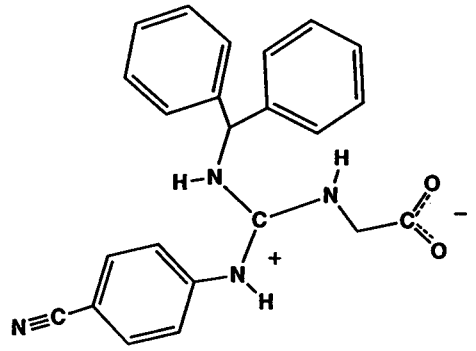

FIGURE 1 Ligand *N*-(*p*-cyanophenyl)-*N'*-(diphenylmethyl)guanidine-acetic acid has a potency more than 200,000 times that of sucrose as assessed by a threshold taste test for sweetness.

kindly provided by Dr. Srinivasan Nagarajan and Dr. Jeff Carter of the NutraSweet Company (Mt. Prospect, IL).

### *Radioligand experiments*

A liquid phase radioimmunoassay for the separation of bound and unbound tritiated ligand was used for detailed ligand binding analysis of the antibody (Kussie et al., 1989). This assay employs 1-ml syringe barrel mini-columns of Sephadex G-25 that separate the mAb-bound ligand from the free ligand containing supernatant. The mAb samples used in these assays were from either hybridoma tissue culture supernatant or hybridoma ascites from which Ig was purified by G-protein affinity chromatography. Titration assays were performed by incubating a single concentration of radio-labeled ligand ([$^3$H]-ligand; 48 Ci/mmol) with serial dilutions of mAb to determine a proper dilution for subsequent saturation assays. Competitive ligand binding experiments with different ligand analogs and $IC_{50}$ determinations were carried out by standard procedures (Kussie et al., 1989). Statistical analyses and plotting of data were accomplished with the programs EBDA and LIGAND (McPherson, 1985).

The radioimmunoassay was used to determine the pH sensitivity of ligand binding to NC6.8. The assay was performed in 0.16-M NaCl containing the following buffers: glycine-HCl buffer (pH 3.3), acetate buffer (pH 4.1 to 5.5), phosphate buffer (pH 6.1 to 7.5), *tris*-HCl buffer (pH 7.8 to 9.1), carbonate buffer (pH 9.5 to 11.2), and phosphate-NaOH buffer (pH 12.0). All assay components ([$^3$H]-ligand and mAb) were diluted in the different buffers and incubated for 2 h at room temperature. The concentration of antibody was sufficient to bind approximately 50% of the [$^3$H]-ligand radioligand. For each buffer, the amount of nonspecific [$^3$H]-ligand binding was obtained in control tubes without mAb.

### *Spectroscopic methods*

Absorption spectral measurements were carried out with a Shimadzu PC2101 UV–Visible double-beam spectrophotometer (Shimadzu Scientific Instruments, Inc., Columbia, MD). The spectra were recorded in the wavelength range of 230–800 nm. A slit width of 2.0 nm and a fast scan were employed. Charge-transfer complex band formation was examined in the absorbancy range of 0.3–0.5 (at 280 nm). Ligand solution was added in microliter quantities to the solution containing mAb NC6.8, starting with the lowest ligand concentration solution first. A spectral scan was carried out after 2 min; the absorbance values did not change with longer reaction time periods. An initial titration was performed to yield 30 data points for a wide concentration range of the ligand before the data were analyzed. Titrations were repeated for 20 data points in the narrow concentration range of interest.

Fluorescence spectral measurements were made with a SLM 8000 spectrofluorimeter (SLM Instruments, Urbana, IL) equipped with a thermostatic cell holder and magnetic stirrer. The excitation wavelength employed was 280 nm, and emission was monitored in the range of 310–370 nm; peak emission was usually near 335 nm. The excitation and emission slit widths were maintained at 4 and 8 nm, respectively. The fluorescence intensities were obtained as the ratio of a fluorescent beam to a straight-through beam to compensate for fluctuations in lamp intensity. Emission intensities at a single wavelength were also collected over a period of 10 s. All spectral data were processed on a microcomputer dedicated to the SLM 8000. We previously described our procedures for corrections of emission intensity to compensate for dilution and photobleaching effects (Droupadi et al., 1993).

A double inverse plot of $\Delta F(F_0 - F_i)$, where $F_0$ and $F_i$ are the fluorescence intensities in the absence and presence of ligand, respectively, near the saturation point versus concentration of the ligand was constructed to yield the maximum fluorescence quenching according to the method of Lehrer (1971). Equilibrium association constants were evaluated according to the method of Stinson and Holbrook (1973) using the equation $1/(1 - q)K_A = [L_i]/q - p[A_i]$, where $q$, the fractional occupancy of binding sites, is given by $\Delta F/\Delta F_{max}$, where $\Delta F_{max}$ is the maximum fluorescence quenching obtained by the double inverse plot, $K_A$ is the intrinsic association constant, $p$ is the number of binding sites, and $L_i$ and $A_i$ are the concentrations of the ligand and the antibody, respectively. The natural logarithm of $K_A$ calculated at different temperatures was plotted against the inverse of absolute temperature (van't Hoff analysis) to evaluate the enthalpic change ($\Delta H = -\text{slope}/R$) involved in the binding process. The change in the free energy ($\Delta G$) of the system was obtained by the equation $\Delta G = -RT \ln K_A$. The change in the entropy ($\Delta S$) of the system was calculated by the equation $\Delta G = \Delta H - T\Delta S$.

## RESULTS

The sequence of NC6.8 was compared against ten antibody sequences with high-resolution structures as shown in Fig. 2 *A* and *B* (Suh et al., 1986; Fischmann et al., 1991; Herron et al., 1989; Kratzin et al., 1989; Lascombe et al., 1992; Padlan et al., 1989; Saul and Poljak, 1992; Sheriff et al., 1987; Strong et al., 1991). For the L chain, the antifluorescein antibody (4FAB) had the highest score of 99, with no deletions or additions required in the loop regions. The next best match was with antibody McPC603 (2MCP) with a score of 70 and a deletion in the CDRL1. There were eleven replacements in the antifluorescein antibody, with four of them in the FR1 and one each in CDR1, CDR2, and the FR3, whereas the FR2 and CDR3 had two replacements each. The statistics for the H chain showed that HyHel-5 antibody (2HFL) had the maximum score of 94, with no deletions or additions required. The next best fit, the anti-arsonate antibody R19.9 (2F19) had a score of 77 and had eight deletions in the CDRH3 loop alone. There were twenty-two replacements in the HyHel-5 antibody, six of which were in the CDR3, five in the FR1, four in the FR3, three in the CDR2, two in FR4, and one each in CDR1 and FR1. Hence, an initial unrefined model was generated using the L chain of 4FAB and the H-chain structure of 2HFL.

The starting model structure had a high-energy configuration of $1.7 \times 10^5$ kcal/mol. The root-mean-square deviation (rmsd) of the model structure against the x-ray native structure showed a deviation of 2.3 Å. This model was then subjected to 200 steps of Powell's energy minimization, resulting in a structure with an energy of $-7.56 \times 10^3$ kcal/mol. The total energy of the structure varied from

**A**

```
L-CHAIN
          1                          CDR1(26-32)                    CDR2(49-56)          70
NC6.8     ELvmtqSplslpvslgdqasiscrPsqslvhs*NqntylhwylqkpgqspklliyRvsnrfsgvpdrfsgsgsgtA
1FDL      diqmtqspaslsasvgetvtitcrasq******nihnylawyqqkqgkspqllvyvtttladgvpsrfsgsgsgtq
2F19      divltqspaslsaslgdrvtiscrasq******disnylnwyqqkpdgtvkliiyvtsrlhsgvpsrfsgsgsgtd
2FBJ      eivltqspaitaaslgqkvtitcsass*******svsslhwyqqksgtspkpwiyeisklasgvparfsgsgsgts
2HFL      divltqspaimsaspgekvtmtcsass*******svnymywyqqksgtspkrwiydtsklasgvpvrfsgsgsgts
2IG2      qsvltqpps*asgtpgqrvtiscsgtssn****igsstvnwyqqlpgmapkllivrdamrpsgvpdrfsgsksgas
2MCP      divmtqspsslsvsagervtmscksqsqllnsgnqknflawyqqkpgqppkllivgastresgvpdrftgsgsgtd
3HFM      divltqspatlsvtpgnsvslscrasq******signnlhwyqqkshesprllikyasqsisgipsrfsgsgsgtd
4FAB      DVvmtqTplslpvslgdqasiscrSsqslvhs*QntylRwylqkpgqspkVliyKvsnrfsgvpdrfsgsgsgtD
6FAB      diqmtqipsslsaslgdrvsiscrasq******dinnflnwyqqkpdgtikliiyftsrsqsgvpsrfsgsgsgtd
7FAB      asvltqpps*vsgapgqrvtisctgsss***nigaghnvkwyqqlpgtapkllifhnn*******arfsvsksgts

          71                  CDR3 (89-97)        106
NC6.8     ftlkisrveaedlgvyfcsqGthvp******Ytfgggtklei
1FDL      yslkinslqpedfgsyycqhfwstp******rtfgggtklei
2F19      ysltisnlehediatyfcqqgstlp******rtfgggtklei
2FBJ      ysltintmeaedaaiyycqqwtypl******itfgagtklel
2HFL      ysltissmetedaaeyycqqwgrnp*******tfgggtklei
2IG2      aslaigglqsedetdyyCaawdvsl****navvfgtgtkvtv
2MCP      ftltissvqaedlavyycqndhsyp******ltfgagtklei
3HFM      ftlsinsvetedfgmyfcqqsnswp******ytfgggtklei
4FAB      ftlkisrveaedlgvyfcsqSthvp******Wtfgggtklei
6FAB      ysltisnleqediatyfcqqgnalp******rtfgggtklei
7FAB      atlaitglqaedeadyycqsydrsl******ryfgggtkltv
```

**B**

```
H-Chain
          1                          CDR1 (26-35)                CDR2 (50-65)          70
NC6.8     RvqlLEsgaelmkpgasvQisckaTgytfsEywiewvkErpghglewigeilp**gsgRtnyReKfkgkatft
1FDL      qvqlkesgpglvapsqslsitctvsgfsltqygvnwvrqppgkglewlgmiw***qdqntdynsalksrlsis
2F19      qvqlqqsgaelvragssvkmsckasgytftsygvnwvkqrpgqglewigyinp**gkqvlsynekfkgkttlt
2FBJ      evkllesggglvqpggslklscaasgfdfskywmswvrqapgkglewigeihp**dsqtinytpslkdkfiis
2HFL      EvqlQQsgaelmkpgasvKisckaSgytfsDywiewvkQrpghglewigeilp**gsgStnyHeKfkgkatft
2IG2      evqlvqsgggvvqpgrslrlscsssgfifssyamywvrqapgkglewvailw**ddgsdqhyadsvkgrftis
2MCP      evklvesggglvqpggslrlscatsgftfsdfymewvrqppgkrlewiaasrnkqnkytteysasvkgrfivs
3HFM      dvqlqesgpslvkpsqtlsltcsvtgdsitsdywswirkfpgnrleymgyvs***vsgstyynpslksrisit
4FAB      evkldetggglvqpgrpmklscvasgftfsdywmnwvrqspekglewvagirnkpynyetyysdsvkgrftis
6FAB      evqlqqsgvelvragssvkmsckasgytftsnqinwvkqrpgqglewigynnp**gngyiaynekfkgkttlt
7FAB      avqleqsgpglvrpsqtlsltctvsgtsfddyystwvrqppgrglewigyvf***ytgttlldpslrsrvtml

          71                          CDR3 (94-102)           113
NC6.8     adtssNtaymqlSsltsedsAvyycTRqYSS***********MdYwgqgtSVtvss
1FDL      kdnsksqvflkmnslhtddtaryycarerdyrl**********dywgqgttltvss
2f19      vdrssstaymqlrsltsedaavyfcarsfyggs****dlavyyfdswgqgttltvss
2FBJ      rdnaknslylqmskvrsedtalyycarlhyygy*********naywgqgtlvtvsa
2HFL      adtssStaymqlNsltsedsGvyycLHqNYD**********FdGwgqgtTLtvss
2IG2      rndskntlflqmdslrpedtgvyfcardgghqfcssascfgp**dywgqgtpvtvss
2MCP      rdtsqsilylqmnalraedtaiyycarnyvgst*******wyfdywgagttvtvss
3HFM      rdtsknqyyldlnsvttedtatyycanwdg*************dywgqgtlvtvsa
4FAB      rddskssvylqmnnlrvedmgiyyctgsyyg***********mdywgqgtsvtvss
6FAB      vdkssstaymqlrsltsedsavyfcarseyygqs*******ykfdywgqgttltvss
7FAB      vntsknqfslrlssvtaadtavyycarnliagc*********idywgqgslvtvss
```

FIGURE 2 (*A*) L-chain V-region sequences of NC6.8 and some of the antibodies that were aligned using the automated antibody structure generation program, ABGEN. The CDR residues are underlined. The conservative replacements are shown in uppercase, and the nonconservative replacements are denoted in boldface uppercase for the parent (4FAB) and model sequences alone. Residues are numbered according to Kabat et al. (1991). (*B*) H-chain V-region sequences of NC6.8 and some of the antibodies that were aligned using ABGEN. The CDR residues are underlined. The conservative replacements are shown in uppercase, and the nonconservative replacements are denoted in boldface uppercase for the parent (2HFL) and model sequences alone. Residues are numbered according to Kabat et al. (1991).

$-7.53 \times 10^3$ to $-7.76 \times 10^3$ kcal/mol during 20 ps of molecular dynamics.

Examination of the CDRs in the native x-ray structure showed that some of the canonical features in CDRs L1 and H1 were not satisfied (these have been discussed in detail below) (Chothia and Lesk, 1987). This prompted us to examine the x-ray structure of NC6.8 with the ligand bound. The rmsd of the main-chain atoms for the L and H chains of the modeled structure with the x-ray (native) were 1.1 and 1.7 Å, those between the liganded form and the model were 1.0 and 1.7 Å, respectively. Phi–psi plots of the L- and H-chain model structures are presented in Fig. 3 *A* and *B*; no abnormal values were noted.

We discuss the comparison of the theoretical model with the x-ray structures for each of the CDR regions (Tables 2 and 3).

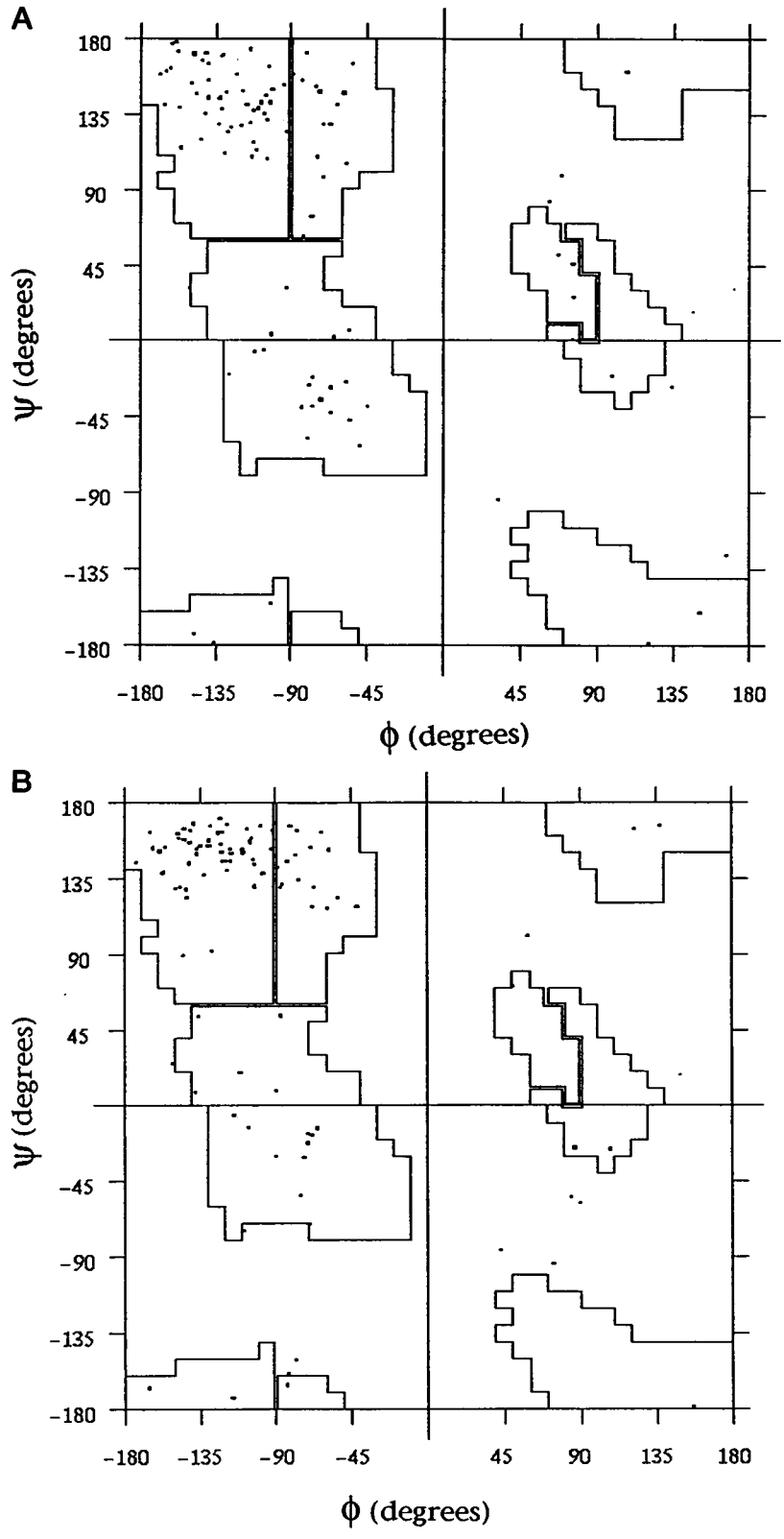


FIGURE 3 (*A*) Phi–psi plot for the NC6.8 model L chain. (*B*) Phi–psi plot for the NC6.8 model H chain.

*L1:* The modeled loop and the liganded x-ray structure are consistent with the canonical structure requirements. H bonds are formed between the main-chain atoms of L:27b and L:32 as also L:27d and L:30. L27b, which is a Leucine, has its side chain pointing into the hydrophobic cavity between the two $\beta$ sheets. However, the native x-ray structure does not satisfy the canonical feature requirement of an H bond between L:27d and L:30. The backbone rmsd of the

**TABLE 2 rmsd of residues in the L-chain CDRs of the model from the x-ray native and complex structures**

| L-CDR1 | | | L-CDR2 | | | L-CDR3 | | |
|---|---|---|---|---|---|---|---|---|
| Residue | rmsd Native | rmsd Complex | Residue | rmsd Native | rmsd Complex | Residue | rmsd Native | rmsd Complex |
| Ser-26 | 2.2 | 1.9 | Tyr-49 | 1.8 | 2.1 | Ser-89 | 1.1 | 1.1 |
| Gln-27 | 1.6 | 1.4 | Arg-50 | 1.8 | 2.2 | Gln-90 | 1.6 | 1.5 |
| Ser-27A | 2.5 | 2.0 | Val-51 | 1.4 | 1.1 | Gly-91 | 1.8 | 2.0 |
| Leu-27B | 1.3 | 1.6 | Ser-52 | 1.2 | 1.0 | Thr-92 | 2.0 | 1.8 |
| Val-27C | 2.2 | 2.4 | Asn-53 | 1.3 | 1.5 | His-93 | 1.1 | 1.4 |
| His-27D | 1.3 | 1.9 | Arg-54 | 2.5 | 1.8 | Val-94 | 3.6 | 4.9 |
| Ser-27E | 2.5 | 1.9 | Phe-55 | 1.7 | 1.6 | Pro-95 | 2.0 | 2.2 |
| Asn-28 | 3.6 | 3.3 | Ser-56 | 1.7 | 0.9 | Tyr-96 | 2.2 | 2.3 |
| Gly-29 | 4.9 | 4.8 | | | | Thr-97 | 1.6 | 1.8 |
| Asn-30 | 4.2 | 4.1 | | | | | | |
| Thr-31 | 1.2 | 1.0 | | | | | | |
| Tyr-32 | 0.9 | 1.7 | | | | | | |
| rmsd back | 1.8 | 1.7 | rmsd back | 0.8 | 0.6 | rmsd back | 0.9 | 0.9 |
| rmsd all | 2.1 | 2.3 | rmsd all | 1.4 | 1.4 | rmsd all | 1.4 | 1.6 |

model from the x-ray native and complex structures is 1.6 and 0.9 Å (Fig. 4A and B), and that for all the atoms is 2.1 and 1.4 Å, respectively, and the rmsd between the native and the complex x-ray structures is 0.5 Å.

*L2:* The backbone rmsd of the model from the native and complex is structures 0.6 and 0.5 Å, respectively (Fig. 4 *A* and *B*), and the total rmsd between the model and each of the x-ray structures is 1.4 Å. The modeled loop satisfies the conformational requirements of a three-residue turn and packing of the FR against the loop residues. Also, as required by the canonical configuration, there is an H bond between the main-chain atoms of L:49 and L:53. Both the native and the liganded structures satisfy the requirements too, with the rmsd between the native and complex crystal structures being 0.4 Å.

*L3:* This nine-residue-long loop maintains all the structural requirements of other canonical L3 configurations in the model and the two x-ray structures. L:95 which is a Pro, is a *cis*-peptide. Also there is a characteristic H bond between the main-chain atoms of L:90 and L:97. A side-chain amide of L:90 forms an H bond with the carbonyls of L:93 and L:95, and the side-chain oxygen forms an H bond with the amide of L:92. The model structure has a backbone rmsd of 0.9 Å and a total rmsd of 1.4 Å (Fig. 4 *A* and *B*) and 1.6 Å with the native and complex structures, respectively. The rmsd between the two crystal structures is 0.4 Å.

*H1:* The backbone rmsd of the modeled structure from the native and complex structures is 1.0 and 0.4 Å (Fig. 4 *C* and *D*). The total rmsd of the model from the native and complex x-ray structure is 2.1 and 2.0 Å. The H1 loop

**TABLE 3 rmsd of residues in the H-chain CDRs of the model from the native and complex structures**

| H-CDR1 | | | H-CDR2 | | | H-CDR3 | | |
|---|---|---|---|---|---|---|---|---|
| Residue | rmsd Native | rmsd Complex | Residue | rmsd Native | rmsd Complex | Residue | rmsd Native | rmsd Complex |
| Gly-26 | 1.9 | 1.9 | Glu-50 | 1.4 | 0.9 | Asp-94 | 2.4 | 2.1 |
| Tyr-27 | 3.6 | 4.1 | Ile-51 | 1.1 | 0.6 | Gly-95 | 1.8 | 2.6 |
| Thr-28 | 2.2 | 2.7 | Leu-52 | 1.9 | 1.9 | Tyr-96 | 4.7 | 4.7 |
| Phe-29 | 1.1 | 1.0 | Pro-52A | 1.9 | 1.8 | Ser-97 | 6.5 | 7.4 |
| Ser-30 | 2.3 | 1.8 | Gly-53 | 1.6 | 2.1 | Ser-98 | 8.9 | 9.1 |
| Glu-31 | 5.5 | 5.0 | Ser-54 | 2.3 | 2.2 | Met-100 | 0.3 | 10.1 |
| Tyr-32 | 2.7 | 2.5 | Gly-55 | 1.8 | 1.7 | Asp-101 | 2.9 | 2.9 |
| Trp-33 | 2.4 | 1.6 | Arg-56 | 6.6 | 6.7 | Tyr-102 | 4.2 | 4.1 |
| Ile-34 | 1.7 | 1.4 | Thr-57 | 2.2 | 2.0 | | | |
| Glu-35 | 1.6 | 2.1 | Asn-58 | 1.7 | 2.0 | | | |
| | | | Tyr-59 | 1.3 | 1.6 | | | |
| | | | Arg-60 | 1.9 | 1.8 | | | |
| | | | Glu-61 | 5.1 | 5.0 | | | |
| | | | Lys-62 | 2.0 | 1.3 | | | |
| | | | Phe-63 | 1.8 | 1.7 | | | |
| | | | Lys-64 | 3.4 | 2.9 | | | |
| | | | Gly-65 | 1.9 | 2.0 | | | |
| rmsd back | 1.1 | 0.8 | rmsd back | 1.2 | 1.2 | rmsd back | 2.4 | 2.7 |
| rmsd all | 2.1 | 2.3 | rmsd all | 2.4 | 2.4 | rmsd all | 3.9 | 3.9 |

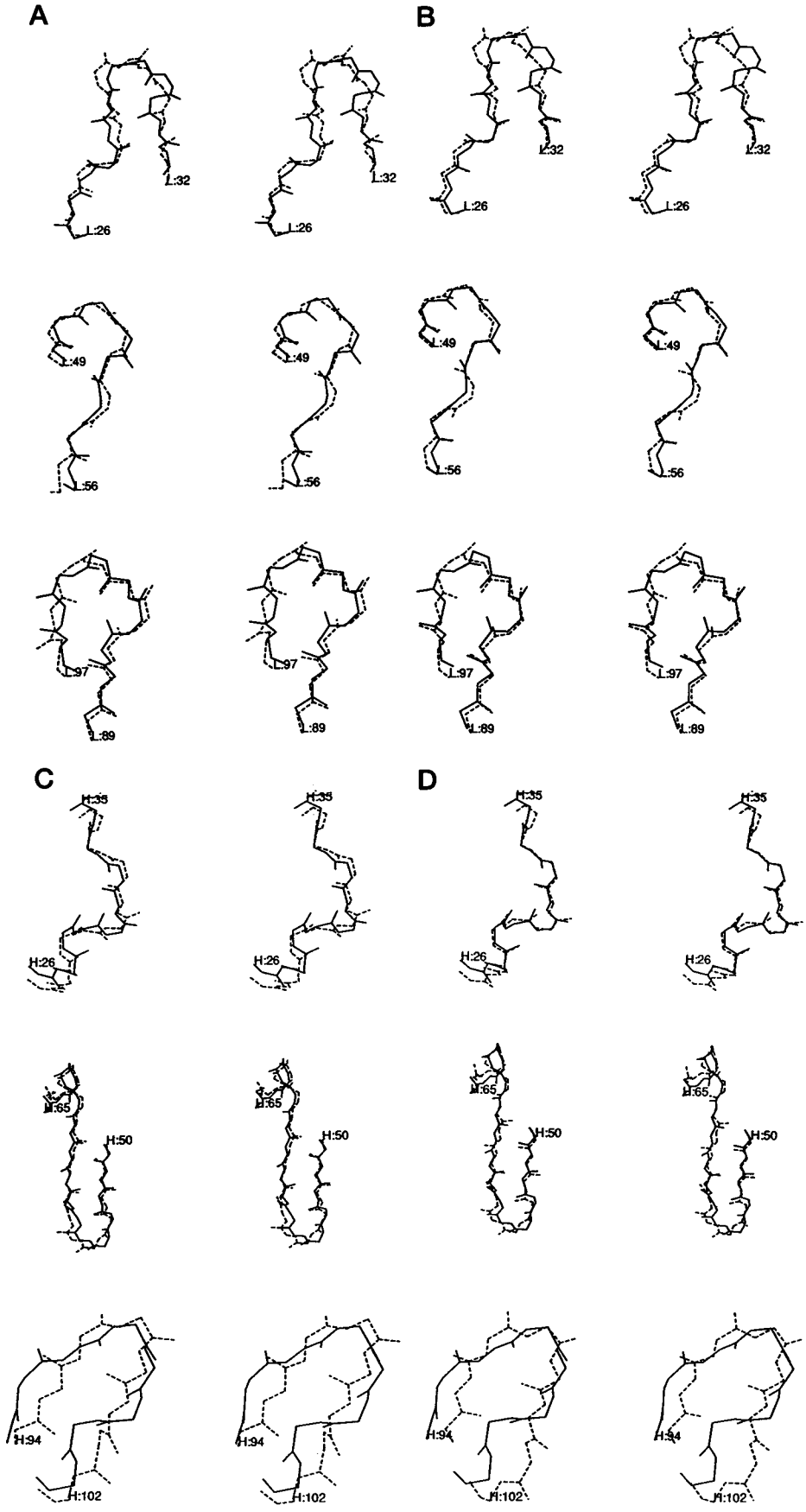


FIGURE 4 (*A*) Stereo drawing of the main-chain atoms for the NC6.8 native x-ray structure (*dashed lines*) and the NC6.8 model (*solid lines*) for the L-chain CDRs. The beginning and ending residues for each loop are numbered according to the system of Kabat et al. (1991). The rmsd from the x-ray structures and canonical features of the loops are discussed in the text and in Table 2. (*B*) Stereo drawing of the main-chain atoms for the NC6.8 with ligand x-ray structure (*dashed lines*) and the NC6.8 model (*solid lines*) for the L-chain CDRs. The beginning and ending residues for each loop are numbered according to the system of Kabat et al. (1991). The rmsd from the x-ray structures and canonical features of the loops are discussed in the text and in Table 2. (*C*) Stereo drawing of the main-chain atoms for the NC6.8 native x-ray structure (*dashed lines*) and the NC6.8 model (*solid lines*) for the H-chain CDR regions. Beginning and ending residues for each loop are numbered according to the system of Kabat et al. (1991). The rmsd from the x-ray structures and canonical features of the loops are discussed in the text and in Table 3. (*D*) Stereo drawing of the main-chain atoms for the NC6.8 with ligand x-ray structure (*dashed lines*) and the NC6.8 model (*solid lines*) for the H-chain CDR regions. Beginning and ending residues for each loop are numbered according to the system of Kabat et al. (1991). The rmsd from the x-ray structures and canonical features of the loops are discussed in the text and in Table 3.

maintains all the canonical features, with the side chain of H:29 buried within the framework and packing against the side chain of H:34. The Gly at H:26, which is conserved, introduces the sharp turn that characterizes the first turn in the H1 loops. In the native structure the distance between the backbone atoms of H:28 and H:31 is too large to form an H bond, which is one of the structural requirements of the canonical feature, whereas the complex x-ray structure satisfies all the canonical requirements. The rmsd between the native and liganded structures is 0.7 Å, with the largest deviation in Glu H:31. This could explain the large deviation between the native and the model structure.

*H2:* The H2 loop is 15 residues long and is very similar to both the x-ray structures, with the backbone rmsd being 0.7 Å (native) and 0.9 Å (complex) (Fig. 4 *C* and *D*) and that between the two x-ray structures being 0.5 Å. The total rmsd of the model from both the native and complex x-ray structures is 2.4 Å. All the canonical requirements are satisfied by all three structures, with the H bonds formed between the main-chain atoms of H:52 and H:56. The loop region from H:52 to H:56 forms part of the four-residue turn described by Chothia and co-workers (Chothia et al., 1989) in which the conformation and position of the four residue regions are determined by the packing against the $V_H$ framework and the identity of the residue at position 71 in particular. H:71 is an Ala, and this packs against H:52a, which is a Pro, causing a change in the conformation of the loop.

*H3:* The H3 loop involved the maximum replacements from the parent model. Of the eight residues in the loop only two were conserved between the two sequences. Also there are no canonical configurations defined for this loop region (Chothia and Lesk, 1987). Hence this gave the maximum deviations from both the native and the complex x-ray structures, with the backbone rmsd being 2.1 and 2.3 Å, respectively (Fig. 4 *C* and *D*) and the rmsd of all the atoms in the model from both of the crystal structures being 3.9 Å. However, the deviation between the two x-ray structures is 0.8 Å.

## Competitive ligand binding experiments

The dissociation constant for NC6.8 with the guanidinium ligand has been determined to be 53 nM (Anchin and Linthicum, 1993). Ligand binding specificity of NC6.8 was determined by examination of different analogs with substitutions at the three major sites (viz., the cyanophenyl group, the carboxymethyl moiety, and the diphenylmethyl system). Analogs with substitutions at the cyanophenyl portion, such as chlorophenyl and azidophenyl, exhibited poor binding ($IC_{50}$ values in excess of 200 mM). Replacement of the acetic acid portion of the ligand with a tetrazolylmethyl significantly reduced binding affinity ($IC_{50}$ = 32 mM). Substitutions of groups such as biphenylmethyl, cyclooctyl, and diethylmethyl for the diphenylmethyl produced only a slight decrease in ligand binding ($IC_{50}$ values ranged from 224 to 750 nM), but these observations are not surprising because the parent ligand was conjugated through the para position of one of the phenyl rings for preparation of the immunogen and it is likely that this region of the ligand would be a minor immunorecognition epitope.

The effects of pH on ligand binding were determined by changes in the solvent pH of the RIA. The aryl nitrogen (adjacent to the cyanophenyl ring) has been determined to have a pKa of 9.3 (M. Sulikowski and D. S. Linthicum, unpublished observations), and thus at pH 7.0 the aryl nitrogen and the guanidinium core carries a delocalized positive charge that may be available for an H bond or a salt bridge with a corresponding site in the antibody.

## Spectroscopic determinations

Absorption and fluorescence spectroscopy were carried out according to the procedures reported elsewhere (Droupadi et al., 1993). Quenching of the intrinsic fluorescence of NC6.8 on addition of increasing quantities of the guanidinium ligand was used to measure several aspects of the molecular complexation. The method of Lehrer (1971) was used to obtain the maximum fluorescence quenching, by plotting the flourescence intensities in the absence and presence of ligand near the saturation point versus the concentration of the ligand. NC6.8 had a maximum emission at 332 nm and a monotonic fluorescence quenching ($Q_{max}$ = 20%) on addition of the ligand (Table 4). There was no energy transfer detectable, and the absorption spectrum of the ligand did not overlap the emission spectrum of mAb.

The magnitude of changes in the emission intensity on association with ligand was related to the concentration of the ligand. Fig. 5 is a titration curve showing the quenching of fluorescence intensity on addition of increasing quantities of the ligand. Maximum changes in relative fluorescence intensity were observed at ligand concentrations in the range of 2–30 nM, and saturation was reached near 130 nM. Equilibrium association constants were evaluated according to the method of Stinson and Holbrook (1973) in which the maximum fluorescence quenching is obtained by the double inverse plot. This value was used to calculate the fractional

**TABLE 4 Spectroscopic and thermodynamic parameters for the mAb NC6.8-ligand complex at 25°C**

| Emission Maximum (nm) | $Q_{max}$ (%) | $K_A$ ($10^7$ L/M) | DG (kcal/mol) | DH (kcal/mol) | DS (cal/mol/K) |
|---|---|---|---|---|---|
| 332 | 20 | 1.6 | −9.8 | −5.5 | 14.6 |

Thermodynamic values were derived by van't Hoff analysis (the plot of ln $K_A$ versus the inverse of absolute of temperature).

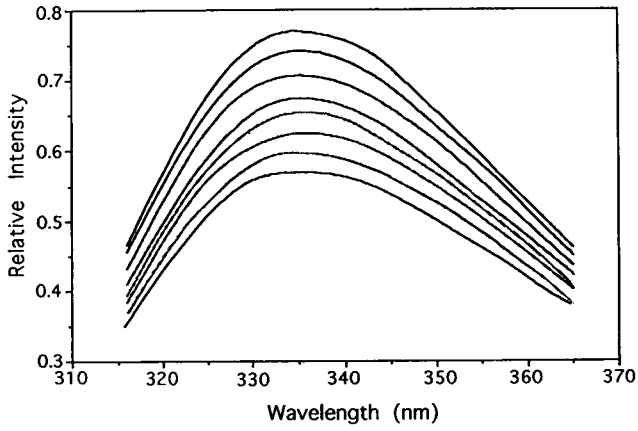


FIGURE 5 Fluorescence emission spectra of the mAb NC6.8 in the presence of increasing concentrations of the guanidinium ligand, from 0 nM (*top curve*) to 130 nM (*bottom curve*), at 25°C in phosphate-buffered saline (ph 7.4).

occupancy of the binding sites. The intrinsic association constant determined by fluoresence quenching were analyzed with the van't Hoff isochore. The slope of the van't Hoff plot corresponds to the enthalpic change involved in the binding of mAb to the ligand. NC6.8 MAb had a positive slope (exothermic); the thermodynamic parameters calculated for the mAb-ligand complex at 25°C are also presented in Table 4.

Absorption spectroscopy of the mAb-ligand complex for NC6.8 and another antisweetener ligand mAb in our collection, NC10.8, was used to identify the presence, if any, of a charge-transfer band resulting from the ligand complexation. Although a strong charge-transfer band was observed for NC10.8, a similar band was not observed for NC6.8 (Fig. 6).

## DISCUSSION

Knowledge-based approaches to antibody modeling use structures from both antigen-bound and antigen-free structures, and therefore it is not obvious whether the modeled structure reflects the sweetener-bound or sweetener-free NC6.8 structure. Inasmuch a high-resolution structures are available for both the bound and the free states (Guddat et al., 1994), comparisons of our model are made against both structures. It should be noted that the above model structure was used in conjunction with experimental studies to predict the ligand binding residues before their elucidation by x-ray crystallography.

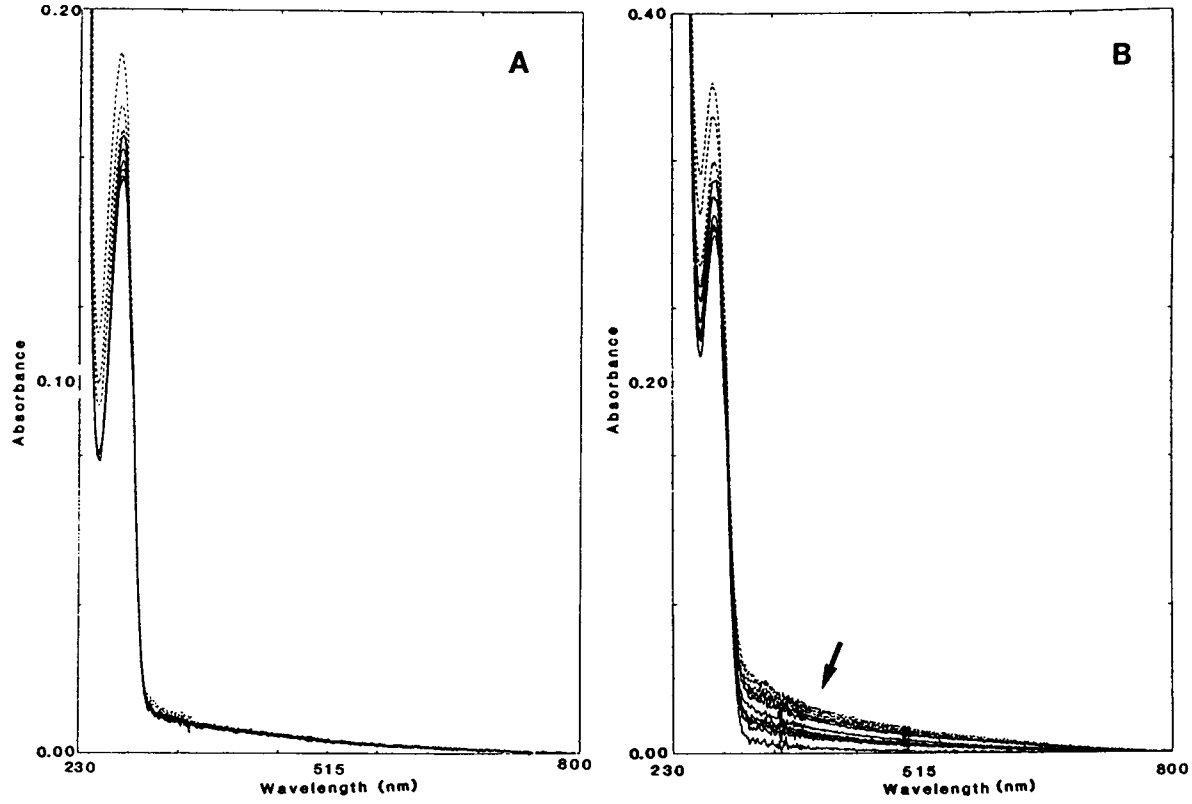


FIGURE 6 (*A*) Absorption spectra of 0.7 mM of mAb NC6.8 in the presence of 0.0, 0.004, 0.012, 0.33, 0.48, 0.90, 1.6, and 2.7 mM of ligand. No increased absorption is observed in the 300–360-nm range. (*B*) Absorption spectra of 1.4 mM of a different mAb (clone NC10.8) in the presence of 0.0, 0.002, 0.05, 0.46, 1.24, 1.95, 2.86, 3.98, and 5.38 mM ligand. The observed increase in absorbance near 260 and 280 nm for both mAb is due to the mAb-ligand complex and free ligand. The increased absorbance in the 300–360-nm range (*arrow*) is attributed to a charge-transfer complex in NC10.8, which is not present in NC6.8.

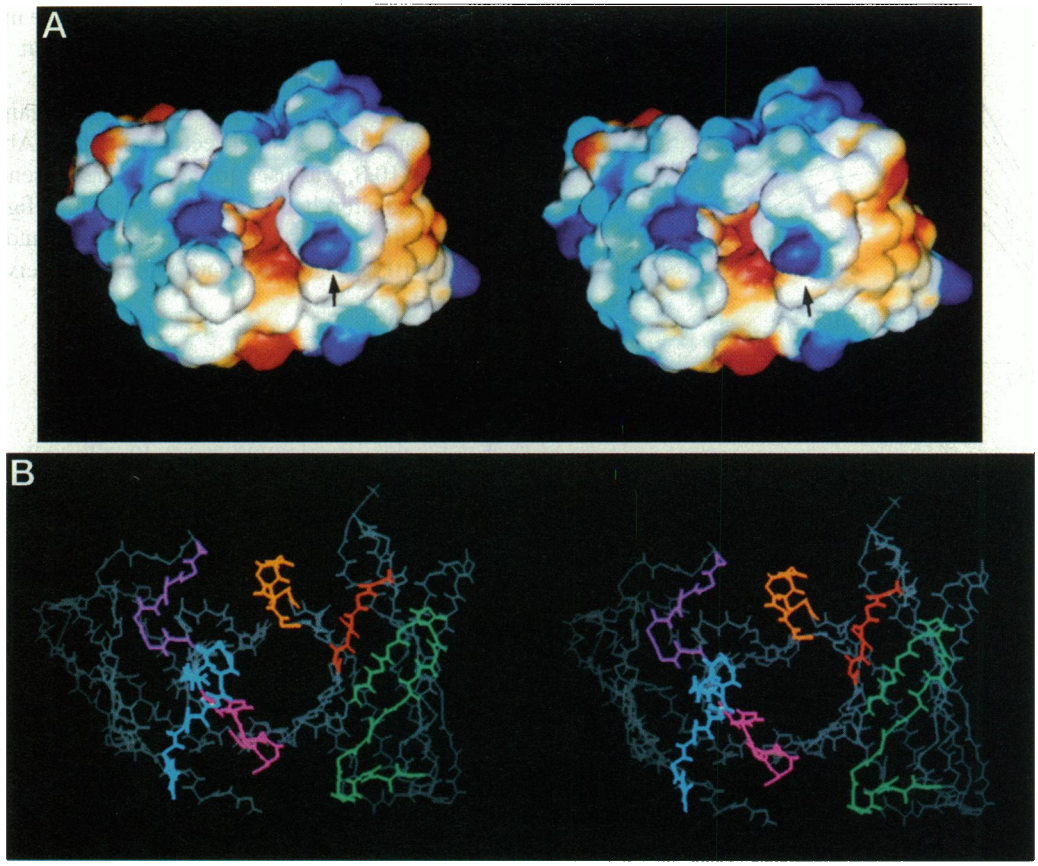


FIGURE 7 (*A*) *En face* stereo rendering of the charges at the van der Waals surface for NC6.8 using the algorithm NCVIEW. The colors are coded according to the Coulombic charges at the van der Waals surface, with blue representing the positively charged potentials and red representing negatively charged potentials; other colors (green, cyan, orange, and yellow) render the gradient between these two extremes. Note the "blue" area (which is due to the side chain of H:56R) at the right of the binding site pocket (*arrow*) and the "red" areas (which are due to the side chains of H:50E and H:35E) down in the ligand binding site (*center*). It is predicted that these three residues interact with the carboxylate and protonated aryl nitrogen of the ligand; the cyanophenyl portion of the ligand is predicted to project down into the antibody pocket. (*B*) *En face* stereo view of the peptide backbone of NC6.8. The CDR are colored as CDRL1 in blue, CDRL2 in pink, CDRL3 in purple, CDRH1 in red, CDRH2 in green, and CDRH3 in orange.

The competitive analog ligand RIA experiments indicated that the binding pocket is very specific for the cyanophenyl moiety of the ligand and cannot accommodate larger or different (in electronic terms) substituents. Furthermore, the carboxylate portion of the ligand was also determined to be a very important feature for antibody recognition. The pH titration experiments suggested that the protonation of the aryl nitrogen of the ligand was also an important feature for antibody recognition. As the pH nears and exceeds the pKa of this nitrogen, the proton is lost, thereby reducing the capacity of the guanidinium to interact with the antibody binding site. The overall "zwitterionic" nature of the ligand has been noted to be an essential characteristic for its intense sweet taste properties (Muller et al., 1992). In contrast to that for the charged portions of the ligand, the nature of the substitutions at the hydrophobic diphenylmethyl system is not so critical for binding to mAb NC6.8. We noted that different hydrophobic substitutions at this site were well tolerated, suggesting that this region of the ligand interacts with hydrophobic residues in the mAb or is pointing out from the central mAb binding pocket. These binding data suggest that the electrostatic nature of both the ligand and the antibody are important factors in ligand recognition.

**TABLE 5 Comparison of key residues predicted to be in contact by ligand binding experiments and modeling with x-ray structure**

| NC174 | Predicted Contact (Experiments and Model)* | X Ray* |
|---|---|---|
| Cyanophenyl | L:34H (vdW) | L:34H (vdW) |
| | L:96Y (vdW) | L:96Y (vdW) |
| | H:35E (vdW) | H:35E (vdW) |
| Biphenyl ring | L:27DH (vdW) | L:27DH (vdW) |
| | L:32Y (vdW) | L:32Y (vdW) |
| | H:96Y (vdW) | H:96Y (vdW) |
| Guanidine group | H:35E (vdW) | H:35E (vdW) |
| | H:50E (vdW) | H:50E (hb,vdW) |
| | | H:96Y (hb,vdW) |
| Carboxy | H:33W (vdW) | H:33W (vdW) |
| | H:56R (hb) | H:56R (hb,vdW) |

* vdW, van der Waals; hb, hydrogen bonding.

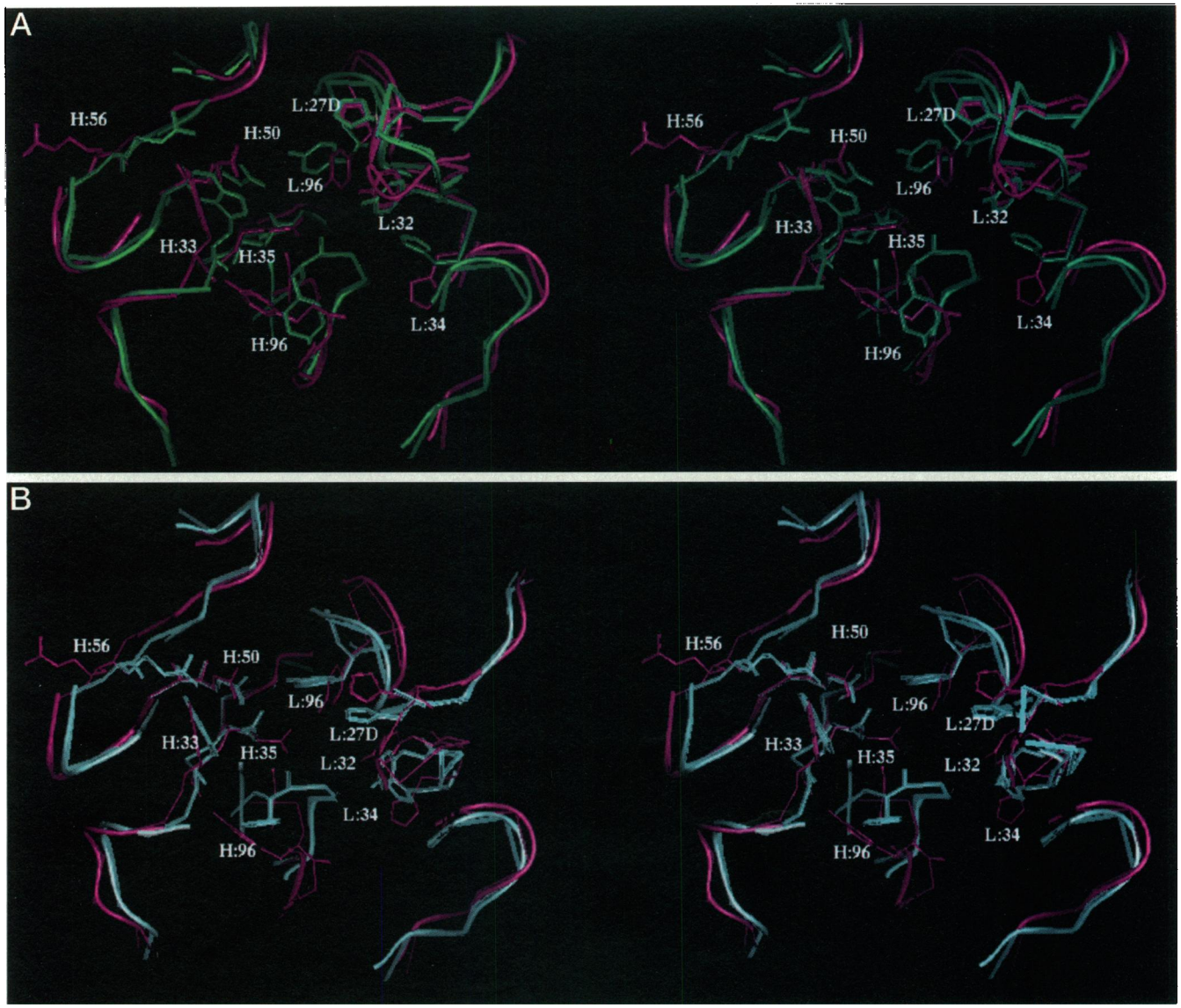


FIGURE 8 (*A*) Stereo drawing of the binding site side chains for the nine residues in the model structure predicted to be involved in ligand recognition with the CDRs (all colored in magenta) compared with their positions in the native x-ray structure (colored in green) NC6.8 Fab. (*B*) Stereo drawing of the binding site side chains for the nine residues in the model structure predicted to be involved in ligand recognition with the CDR regions (all colored in magenta) compared with their positions in the x-ray structure (colored in cyan) of the liganded NC6.8 Fab.

Inspection of the NC6.8 Fv model reveals two acidic residues, H:35E and H:50E, deep in the putative ligand binding pocket. These are predicted to provide a negative electrostatic potential for complementary charge interactions with the positive guanidinium group of the ligand. Fig. 7 *A* shows the stereo *en face* graphical rendering of the electrostatic surface of the NC6.8 Fv model obtained with the NCVIEW algorithm (Purvis and Culberson, 1986). The negatively charged contours (colored in red in the center pocket) highlight the predicted H:50E and H:35E charge interaction sites. Another predicted site for ligand recognition is the basic residue H:56R (CDR2 of the H chain, seen in Fig. 7 *A* in blue), which interacts with the carboxylate moeity of the ligand through the formation of a salt bridge.

Based on this Fv model and ligand binding data, the cyanophenyl portion of the ligand is predicted to point down into the pocket (Fig. 7 *B*). To determine whether Trp residues participate in the ligand recognition we examined the mAb-ligand complex for steady-state quenching of intrinsic Trp fluorescence. We observed an isotonic quenching (i.e., no hypsochromic shift), suggesting the participation of a Trp that is not highly exposed to solvent. NC6.8 has five V-region Trp residues. Four of these, H:36W, H:47W, H:103W, and L:35W, appear in 92–99% of all known murine V-region antibody sequences. The high degree of conservation of these residues suggests a structural role for them. It is unlikely that these are involved in the quenching reaction because of their packing interactions and deep

buried positions relative to the binding pocket. In sharp contrast, the Trp located at H:33 is found in only 3% of known antibody sequences. This Trp is in the combining site as observed in other emperically solved Fab structures (Herron et al., 1989; Sheriff et al., 1987). Based on these observations, we predict that H:33W in mAb NC6.8 is involved in the complexation with the ligand and responsible for the observed ligand-induced fluorescence quenching. The absence of a blue shift in the fluorescence quenching supports the deep-pocket location of this residue in the model.

We used data from absorption spectroscopy to determine whether a charge transfer band could be observed in the mAb-ligand complex. We have observed this type of spectral feature in other NC mAb-ligand complexes (e.g., NC10.8) and have attributed the observed charge-transfer band to the formation of a $\pi$–$\pi$ interaction between an electron-rich donor Trp in the mAb and the electron-poor cyanophenyl ring of the ligand (Anchin and Linthicum, 1993). In the case of NC6.8 we predict that the cyanophenyl ring ligand does not undergo a $\pi$–$\pi$ stacking arrangement with H:33W, because of the absence of any observable charge-transfer band.

The model structure suggests the role of several polar interactions in ligand binding. This in turn would lead to large enthalpic contributions to thermodynamics of binding of the ligand to the antibody. We examined the NC6.8-ligand complexation at different temperatures to evaluate the thermodynamic parameters that govern the association process. The intrinsic association constant corresponds to the free energy changes as calculated by the van't Hoff analysis. This analysis shows that the interaction for this mAb is enthalpically driven (P. R. Droupadi and D. S. Linthicum, unpublished results).

Based on the modeled Fv fragment and experimental studies of ligand binding, we have predicted the identity and position of several key residues responsible for ligand recognition and binding (Table 5). Fig. 8 *A* shows a stereo drawing of the nine residues predicted by the modeling, compared with their positions in the native Fab x-ray structures. Fig. 8 *B* shows the nine residues predicted compared with the ligand-complex mAb. As is apparent from Fig. 8 *A* and *B*, H:33W (observed in ligand-induced fluorescence quenching), the negatively charged residues H:35E and H:50E (which provide the negatively charged environment for the guanidinium moeity in the ligand), H:56R (which provides the counterion for the acetic acid moeity), and L:34H deep in the binding pocket (which is in contact with the cyanophenyl group of the ligand) are identified as key residues involved in antigen binding.

In summary, the combination of computer-aided molecular modeling, competitive analog ligand binding, and fluorescence spectroscopy can facilitate the prediction of the antigen combining sites on an antibody, as demonstrated in this study. Additional experimental and theoretical studies involving this and other high-affinity mAb with the superpotent guanidinium sweeteners are currently under way.

This work was supported by research grant GM46535 from the National Institutes of Health. The computational resources were provided by the National Center for Supercomputing Applications. This study was part of a collaborative research agreement with the NutraSweet Co. (Mt. Prospect, IL), and we thank Drs. Grant DuBois, Mike Kellogg, Srinivasan Nagarajan, Jeff Carter, Chris Culberson, and Eric Walters for their helpful discussions and gift ligands used in this study. We thank Dr. Culberson for allowing us to use the algorithm NCVIEW for these studies.

## REFERENCES

Anchin, J. M., and D. S. Linthicum. 1993. Variable region sequence and characterization of monoclonal antibodies to a *N,N′,N″*-trisubstituted guanidine high, potency sweetener. *Mol. Immunol.* 30:1463–1471.

Anchin, J. M., S. Subramaniam, and D. S. Linthicum. 1991. Binding of the neuroleptic drug Haloperidol to a monoclonal antibody: refinement of the binding site molecular model using canonical structures. *J. Mol. Recog.* 4:7–15.

Bassolino-Klimas, D., R. E. Bruccoleri, and S. Subramaniam. 1992. Modeling the antigen combining site of an anti-dinitrophenyl antibody ANO2. *Protein Sci.* 1:1465–1476.

Bondi, A. 1964. Van der Waals volumes and radii. *J. Phys. Chem.* 68: 441–451.

Bruccoleri, R., E. Haber, and J. Novotny. 1988. Structure of antibody hypervariable loops reproduced by a conformational search algorithm. *Nature (London).* 335:564–568.

Bruccoleri, R. E., and M. Karplus. 1987. Prediction of the folding of short polypeptide segments by uniform conformational sampling. *Biopolymers.* 46:137–168.

Brunger, A. T., J. Kuriyan, and M. A. Karplus. 1987. Crystallographic R-factor refinement by molecular dynamics. *Science.* 235:458–460.

Chothia, C., and A. M. Lesk. 1987. Canonical structures for the hypervariable regions of immunoglobulins. *J. Mol. Biol.* 196:901–917.

Chothia, C., A. M. Lesk, A. Tramontano, M. Levitt, S. J. Smith-Gill, G. Air, S. Sheriff, E. A. Padlan, D. Davies, W. R. Tulip, P. M. Colman, S. Spinelli, P. M. Alzari, and R. J. Poljak. 1989. Conformations of immunoglobulin hypervariable regions. *Nature (London).* 342:877–883.

Chothia, V., A. Lesk, M. Levitt, A. Amit, R. Mariuzza, S. Phillips, and R. Poljak. 1986. The predicted structure of immunoglobulin D1.3 and its comparison with the crystal structure. *Science.* 233:755–758.

Chothia, C., J. Novotny, R. Bruccoleri, and M. Karplus. 1985. Domain association in immunoglobulin molecules. *Mol. Biol.* 186:651–663.

Davies, D. R., and H. Metzger. 1983. Structural basis of antibody function. *Annu. Rev. Immunol.* 1:87–117.

Davies, D. R., E. A. Padlan, and S. Sheriff. 1990. Antibody-antigen complexes. *Annu. Rev. Biochem.* 59:439–473.

de la Paz, P., B. Sutton, M. Darsley, and A. Rees. 1986. Modelling of the combining sites of three anti-lysozyme monoclonal antibodies and of the complex between one of the antibodies and its epitope. *EMBO.* 5:415–425.

Droupadi, P. R., J. M. Anchin, E. A. Meyers, and D. S. Linthicum. 1993. Spectrofluorimetric study of the intermolecular complexation of monoclonal antibodies with the high potency sweetener *N*-(*p*-cyanophenyl)-*N′*-(diphenylmethyl)guanidineacetic acid. *J. Mol. Recog.* 5:173–179.

Fischmann, G. A., G. A. Bentley, T. N. Bhat, G. Boulot, R. A. Mariuzza, S. E. Phillips, D. Tello, and R. J. Poljak. 1991. Crystallographic refinement of the three dimensional structure of the FAB*D1.3-*lysozyme complex at 2.5 Angstrom resolution. *J. Biol. Chem.* 266:12915.

Guddat, L., L. Shan, J. Anchin, D. S. Linthicum, and A. B. Edmundson. 1994. Local and transmitted conformational changes on complexation of an anti-sweetener Fab. *J. Mol. Biol.* 236:247–274.

Herron, J. N., X. He, M. L. Mason, E. W. Voss, and A. B. Edmundson. 1989. Three-dimensional structure of a fluorescein-Fab complex crystallized in 2-methyl-2,4-pentanediol. *Proteins.* 5:271–280.

Jackson, T., B. A. Morris, A. C. R. Martin, D. F. V. Lewis, and P. G. Sanders. 1992. Molecular modelling and site-directed mutagenesis on a bovine anti-testosterone monoclonal antibody. *Prot. Eng.* 5:343–350.

Kabat, E. A., T. T. Wu, H. M. Perry, K. S. Gottesman, and C. Foeller. 1991. Sequences of Proteins of Immunological Interest, 5th ed, NIH

Publication 91–3242. U.S. Department of Health and Human Services, Washington, D.C.

Kratzin, H. D., W. Palm, M. Stangel, W. E. Schmidt, J. Freidrich, and N. Hilschmann. 1989. Dir primaerstructur des kristallisierbaren monoklonalen immunoglobulins IGg 1 = KOL/II aminosaeuresequenz der l-kette, Lambda typ, subgruppe I (German), *Biol. Chem. Hoppe-Seyler.* 370:263.

Kussie, P. H., G. Albright, and D. S. Linthicum. 1989. Production and characterization of monoclonal idiotypes and anti-idiotypes for small ligands. *Meth. Enzymol.* 178:49–63.

Kussie, P. H., J. M. Anchin, S. Subramaniam, J. Glasel, and D. S. Linthicum. 1991. Molecular analysis of the binding site architecture of monoclonal antibodies to morphine by using competitive ligand binding and molecular modelling. *J. Immunol.* 146:4248–4257.

Lascombe, M. B., P. M. Alzari, and A. Poljak. 1992. Three dimensional structure of two crystal forms of Fab R19.9, from a monoclonal anti-arsonate antibody. *Proc. Natl. Acad. Sci. USA.* 89:9429–9433.

Lehrer, S. S. 1971. Solute perturbations of protein fluorescence. The quenching of the tryptophan fluorescence of model compounds and of lysozyme by iodide ion. *Biochemistry.* 25:4602–4609.

Martin, A. C., J. C. Cheethman, and A. R. Rees. 1989. Modeling antibody hypervariable loops: a combined algorithm. *Proc. Natl. Acad. Sci. USA,* 86:9268.

McPherson, G. A. 1985. Kinetic, Ebda, Ligand, and Lowry. A Collection of Radioligand Binding Analysis Programs. Elsevier Science Publishers, Amsterdam, The Netherlands.

Muller, G. W., D. E. Walters, and G. E. DuBois. 1992. *N,N'*-Disubstituted guanidine high-potency sweeteners. *J. Med. Chem.* 35:740–743.

Padlan, E. A. 1990. On the nature of antibody combining sites: unusual structural features that may confer on these sites an enhanced capacity for binding ligands. *Proteins.* 7:112–124.

Padlan, E. A., G. H. Cohen, and D. R. Davies. 1985. On the specificity of antibody-antigen interactions: phosphocholine binding to McPC603 and the correlation of three-dimensional structure and sequence data. A *Inst. Pasteur/Immunol.* 136C:271–276.

Padlan, E. A., E. W. Silverton, S. Sheriff, G. H. Cohen, S. J. Smith-Gill, and D. R. Davies. 1989. Structure of an antibody-antigen complex. Crystal structure of the Hy/Hel-10 Fab-lysozyme complex. *Proc. Natl. Acad. Sci. USA.* 86:5938.

Poljak, R. J., L. M. Amzel, B. L. Chen, Y. Y. Chiu, R. P. Phizacherley, F. Saul, and X. Ysern. 1976. Three-dimensional structure and diversity of immunoglobulins. *Cold Spring Harbor Symp. Quant. Biol.* 41:639–645.

Purvis, G. D., and J. C. Culberson. 1986. On the graphical display of molecular electrostatic force-fields and gradients of the density. *J. Mol. Graphics* 4:88–92.

Saul, F. A., and R. J. Poljak. 1992. Crystal structure of human immunoglobulin fragment Fab NEW refined at 2.0 Angstrom resolution. *Proteins.* 14, 363.

Sheriff, S., E. W. Silverton, E. A. Padlan, G. H. Cohen, S. J. Smith-Gill, B. C. Finzel, and D. R. Davies. 1987. Three-dimensional structure of an antibody-antigen complex. *Proc. Natl. Acad. Sci. USA.* 84:8075–8079.

Sherman, M., and M. Bolger. 1988. Haloperidol binding to monoclonal antibodies. Predictions of three-dimensional combining site structure via computer modeling. *J. Biol. Chem.* 263:4064–4074.

Stinson, R. A., and J. J. Holbrook. 1973. Equilibrium binding of nicotinamide nucleotides to lactate dehydrogenases. *Biochem. J.* 131: 719–728.

Strong, R. K., R. Campbell, D. R. Rose, G. A. Petsko, J. Sharon, and M. N. Margolies. 1991. Three-dimensional structure of murine anti-p-azophenylarsonate Fab 36–71. x-ray crystallography, site-directed mutagenesis, and modeling of the complex with hapten. *Biochemistry.* 30:3739.

Suh, S. W., T. N. Bhat, M. A. Navia, G. H. Cohen, D. N. Rao, S. Rudikoff and D. R. Davies. 1986. The Galactin-*binding immunoglobulin FAB J539. An x-ray diffraction study at 2.6-*angstroms resolution. *Proteins.* 1:74–80.

Tramontano, A., and A. M. Lesk. 1992. Common features of the conformations of antigen-binding loops in immunoglobulins and application to modeling loop conformations. *Proteins.* 13:231–245.